Surfaces and Interfaces 46 (2024) 104023

Contents lists available at ScienceDirect

Surfaces and Interfaces

journal homepage: www.sciencedirect.com/journal/surfaces-and-interfaces

The surface softening mechanism of AlN ceramic by laser treatment

Lingda Xiong [a], Chunjin Wang [a,*], Wei Wu [a], Linjiang Xu [b], Chunming Wang [b], Hui Deng [c], Chi Fai Cheung [a,*]

[a] State Key Laboratory of Ultra-precision Machining Technology, Department of Industrial and Systems Engineering, The Hongkong Polytechnic University, Hung Hom, Hong Kong, China
[b] School of Material Science and Engineering, Huazhong University of Science & Engineering, 430074 Wuhan, PR China
[c] Department of Mechanical and Energy Engineering, Southern University of Science and Technology, No. 1088, Xueyuan Road, Shenzhen, Guangdong, China

ARTICLE INFO

Keywords:
AlN ceramic
Laser
Surface softening mechanism
Hardness variation
Phase transition

ABSTRACT

Aluminum Nitride ceramic is an excellent material for heat dissipation in electronic applications. The precision machining of AlN ceramic is difficult due to its high hardness and brittleness. To improve the machinability of the ceramic material, a microsecond laser was applied to soften the surface of AlN ceramic in this work. To reveal the surface softening mechanism of the laser processing of AlN ceramic, the phase composition, microstructure, processing depth and hardness variation of laser-treated AlN ceramic surface were studied. The phase transition and surface morphology evolution during laser treatment were explained. It was found that Al and Al_2O_3 were formed on the surface after laser treatment. The surface hardness decreased from 14.3 GPa (base material) to 0.708 GPa. The revealed surface softening mechanism of laser treatment in this work is helpful for the optimization of the softening process and post-machining quality.

1. Introduction

Aluminum Nitride (AlN) ceramic is characterized by its high thermal conductivity (greater than 175 W/(m*k) at 25 °C), high electrical resistivity, low thermal expansion coefficient and non-toxic. As a result, it is widely used as substrate materials for high-power electronic devices [1–4]. However, traditional machining of AlN ceramic is found to be problematic because of its high hardness and brittleness. The cutting forces generated in traditional machining of AlN ceramic cause surface or subsurface cracks, which are harmful to AlN ceramic reliability and service life [5–7]. Therefore, it is essential to develop a method to avoid crack formation during the machining process of AlN ceramic [6,8].

In recent years, surface softening was applied to improve the machinability of hard and brittle materials (such as reaction-bonded SiC, single-crystal SiC and WC, etc) [9,10]. Zhang et al. [11] investigated the in-situ laser-assisted diamond cutting of reaction-bonded SiC. They found the hardness of SiC decreased by the in-situ laser heating. The surface softening led to the plastic deformation of material during the cutting process, which was conducive to the formation of high surface quality. Yan et al. [12] applied electrical discharge machining (EDM) before the grinding of single-crystal SiC. The SiC decomposed into Si and C to form a recasting layer during EDM, which increased the material removal rate for the grinding. You et al. [13] studied the laser-assisted diamond turning of binderless WC. They found the WC hardness decreased when the WC was heated by laser. The residual stress of the machined workpiece could be decreased by 40 % with laser assistance.

AlN ceramic decomposes into Aluminum (Al) and Nitrogen(N_2) at high temperature [14–17]. This reaction is called 'metallization'. The surface hardness decreases due to the formation of an Al layer on the AlN ceramic surface. Surface metallization is a promising method to decrease the cutting forces and avoid crack formation during the machining of AlN ceramic. As a heat-concentrated source, laser is widely used in surface treatment, such as laser cleaning, laser polishing, laser drilling, etc. [18–21]. The laser process is a non-contact and highly selective process. It can provide localized treatment and precise control for producing complex features with minimal thermal effect on the bulk material [22–25]. Therefore, laser is thought to be a suitable heat source to achieve the surface metallization of AlN ceramic.

Some research has been conducted to study the laser treatment on AlN ceramic surface. Hirayama et al. [26] applied microsecond (ms), nanosecond (ns) and femtosecond (fs) laser ablations on AlN surface. They found an Al layer was formed on the surface after the microsecond and nanosecond laser-induced thermal decomposition process. However, the nonthermal process occurred with the fs laser ablation. No

* Corresponding author.
E-mail addresses: chunjin.wang@polyu.edu.hk (C. Wang), benny.cheung@polyu.edu.hk (C.F. Cheung).

https://doi.org/10.1016/j.surfin.2024.104023
Received 24 August 2023; Received in revised form 6 January 2024; Accepted 30 January 2024
Available online 1 February 2024

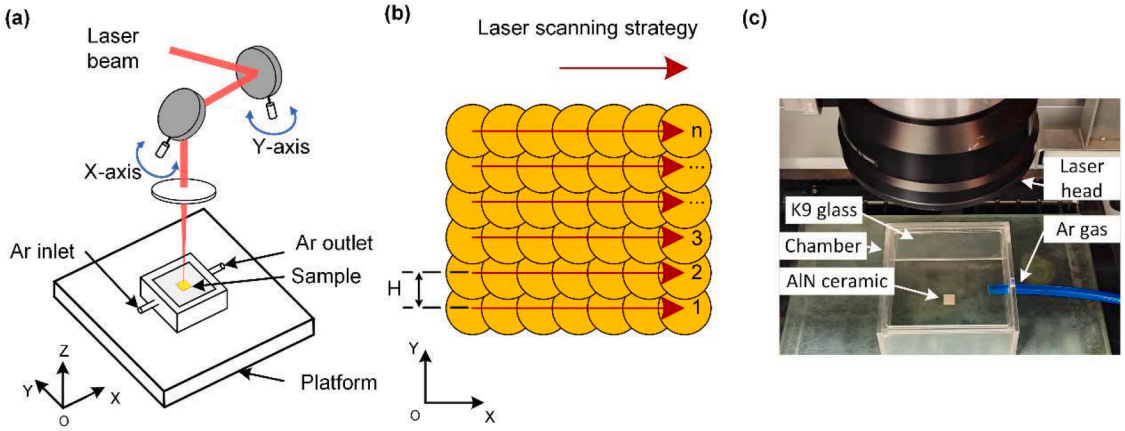

Fig. 1. The schematic diagram of laser treatment experiment: (a) processing diagram (b) laser scanning strategy (c) experimental setup.

Table 1
Experiment parameters of laser treatment.

Sample	*P*(W)	*f*(Hz)	*V*(mm/s)	*H*(μm)	*Ox*	*Oy*
1	40	5000	85	17	82.5%	82.5%
2			127.5	25.5	73.8%	73.8%
3			170	34	65.1%	65.1%
4			212.5	42.5	56.4%	56.4%
5			255	51	47.7%	47.7%
6			297.5	59.5	39.0%	39.0%
7			340	68	30.2%	30.2%

decomposition reaction occurred. The influence of laser parameters on surface metallization was also investigated. Four laser wavelengths of ns laser (266 nm, 355 nm, 532 nm and 1064 nm) were used by Nedyalkov et al. [27] in the experiment of AlN surface metallization by laser. A special ripple structure was formed in the case of irradiation at 1064 nm. Such structure was not observed after laser ablation with the other wavelengths. The influence of pulse duration on AlN surface metallization by laser was investigated by Yang et al. [28]. They found the amount of Al increased with the pulse duration due to increasing thermal diffusion time and depth. The influence of processing parameters on surface metallization was also investigated. The critical laser fluence of KrF excimer laser (wavelength: 248 nm) for surface metallization was 2.0 J/cm^2 while the critical laser fluence of Ytterbium pulsed fiber laser (wavelength: 1064 nm) for surface metallization was 21.53 J/cm^2 [29–31]. Besides, the amount of decomposed Al increased with the number of pulses irradiated at the same position corresponding to a higher amount of absorbed laser energy [32]. AlN surface metallization experiments by laser under different shielding gas environments (air, Ar and N_2) was conducted by Shao et al. [2] They found the critical laser fluences required for AlN decomposition under different shielding gas environment were different.

However, the main purpose of the above works was to improve the electrical conductivity of AlN ceramic by forming a conductive Al layer on AlN surface in high-power electronic devices. The most concerned property of the above works was electrical resistance. Only a conductive Al line or groove was fabricated in most of the above works. There is still a lack of study about the influence of 2-D surface laser treatment on the hardness variation of AlN surface, which is related to the machinability of AlN ceramic. Besides, the influences of process parameters on microstructure and surface roughness were also not clear to date.

Based on the above research background, the 2-D laser surface treatment experiment was conducted in the present work. To reveal the

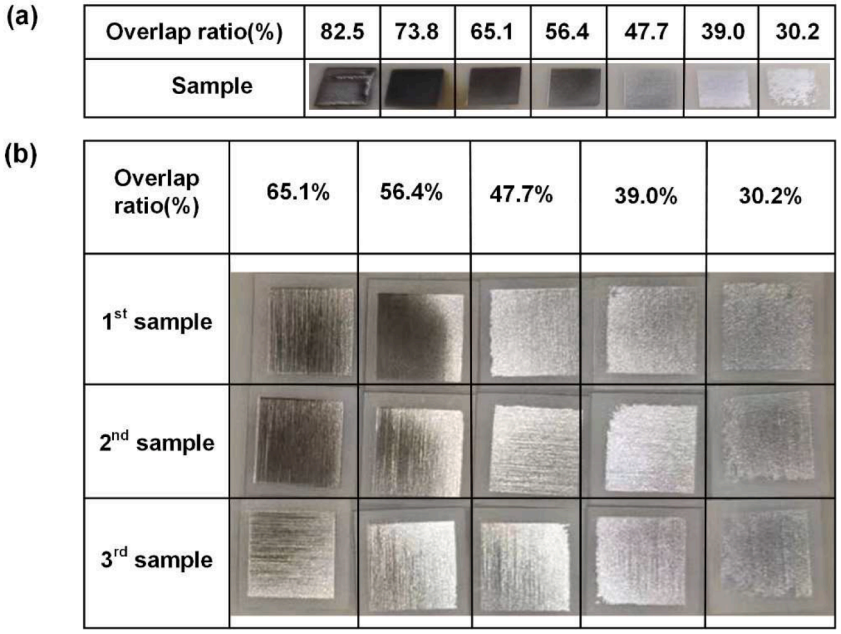

Fig. 2. Macro-morphology of laser-treated surfaces.

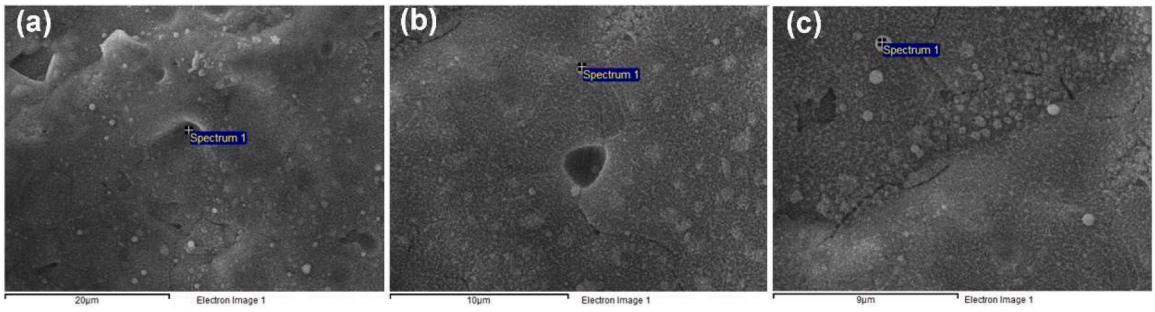

element	Weight (%)	Atomic (%)
Al	100	100%

element	Weight (%)	Atomic (%)
O	35.19	47.80
Al	64.81	52.20

element	Weight (%)	Atomic (%)
O	45.08	58.06
Al	54.92	41.94

Fig. 3. The chemical composition of laser-treated surface at different positions.

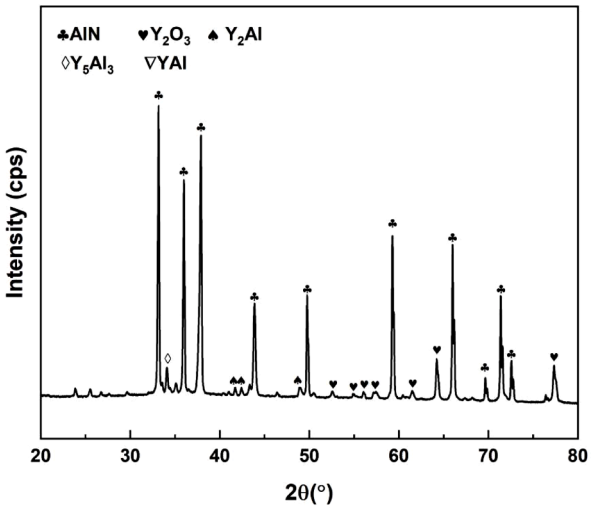

Fig. 4. The XRD spectrum of AlN ceramic.

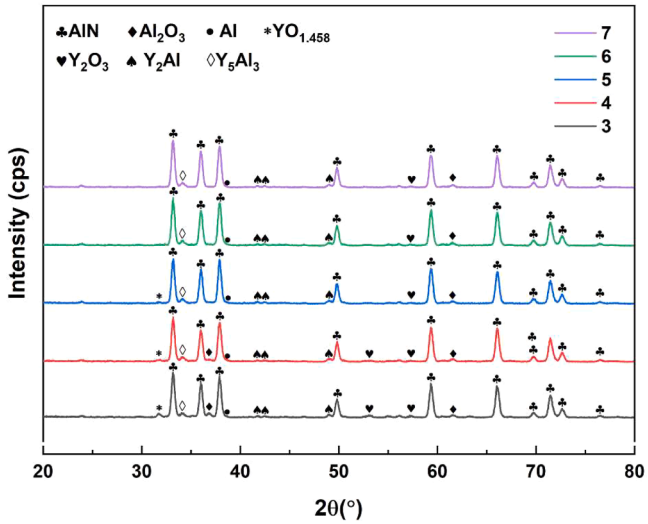

Fig. 5. XRD spectrums of AlN laser-treated surfaces.

AlN ceramic surface softening mechanism by laser irradiation, the phase composition, microstructure and surface roughness of metallized layer and the unmetallized AlN surface beneath the metallized layer were

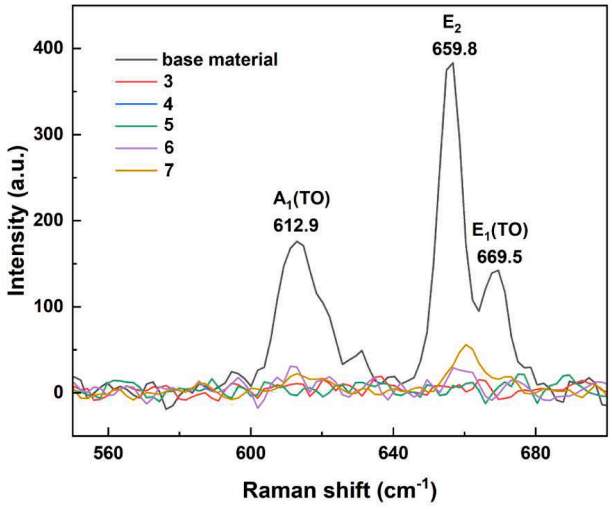

Fig. 6. Raman spectrums of base material and laser-treated surface with different overlap ratios.

observed. Besides, the processing depth and hardness of laser-treated surface were measured after laser treatment. Finally, the formation mechanism of softened surface layer (the metallized layer) was discussed.

2. Experimental details

2.1. Materials

The samples used in the laser treatment experiments were AlN ceramic plates (Feida Electronics Co. Ltd) with the size of 10 mm × 10 mm × 1 mm (thickness). The ceramic was composed of 95 % AlN particles and 5 % Y_2O_3 particles as binders. The surface roughness Sa of AlN ceramic plate ranged from 0.25 μm to 0.5 μm. Before the laser treatment experiments, each plate was cleaned in 99.9 % alcohol by ultrasonic cleaner for 5 minutes.

2.2. Experimental setup

RFL-QCW150 fiber laser (wavelength: 1080 nm) was used in the laser treatment experiment. The laser beam was a Gaussian beam. The schematic diagram of laser treatment was shown in Fig. 1. The AlN sample was placed in a chamber which was filled with Argon (Ar) to protect the metallized surface from oxidation. A K9 glass was placed on the top of chamber to let the laser pass through. The laser was controlled

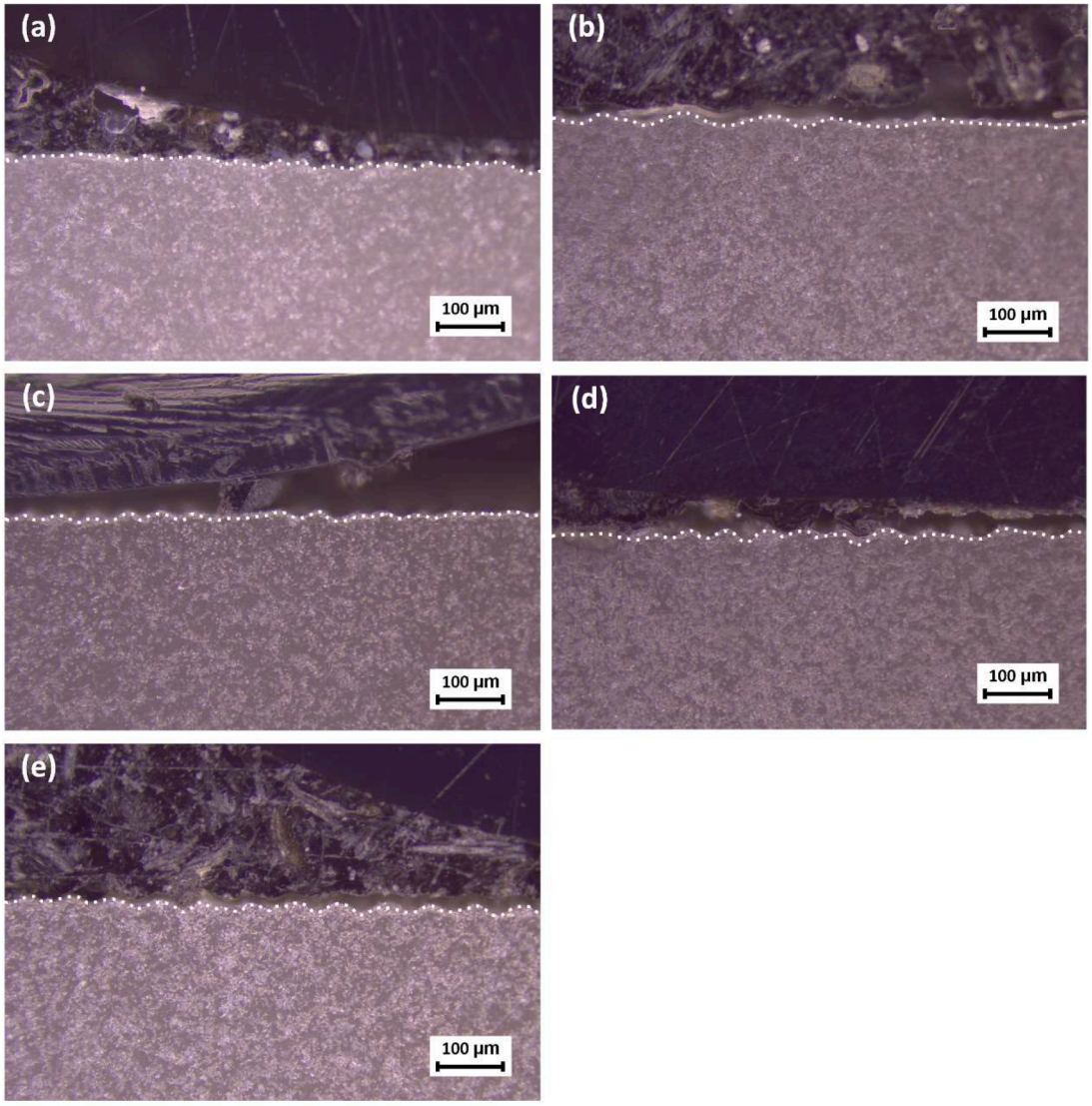

Fig. 7. The cross-section morphologies of laser-treated surfaces: (a) sample 3 with overlap ratio 65.1%, (b) sample 4 with overlap ratio of 56.4%, (c) sample 5 with overlap ratio of 47.7%, (d) sample 6 with overlap ratio of 39.0%, € sample 7 with overlap ratio of 30.2%.

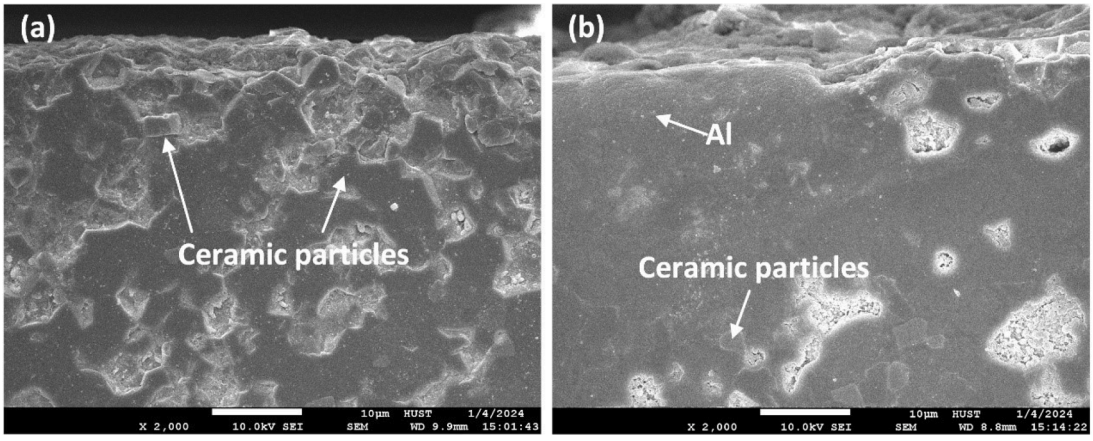

Fig. 8. The surface microstructure of: (a) AlN ceramic, (b) the laser-treated surface.

by a galvanometer scanner to achieve 2-D laser scanning. In the experiment, the laser scanned in the strategy as shown in Fig. 1b. The X direction was the laser scanning direction. The Y direction was vertical to the laser scanning direction.

Preliminary experiments were done to determine the appropriate laser fluence which was defined as the quotient of the pulse energy and

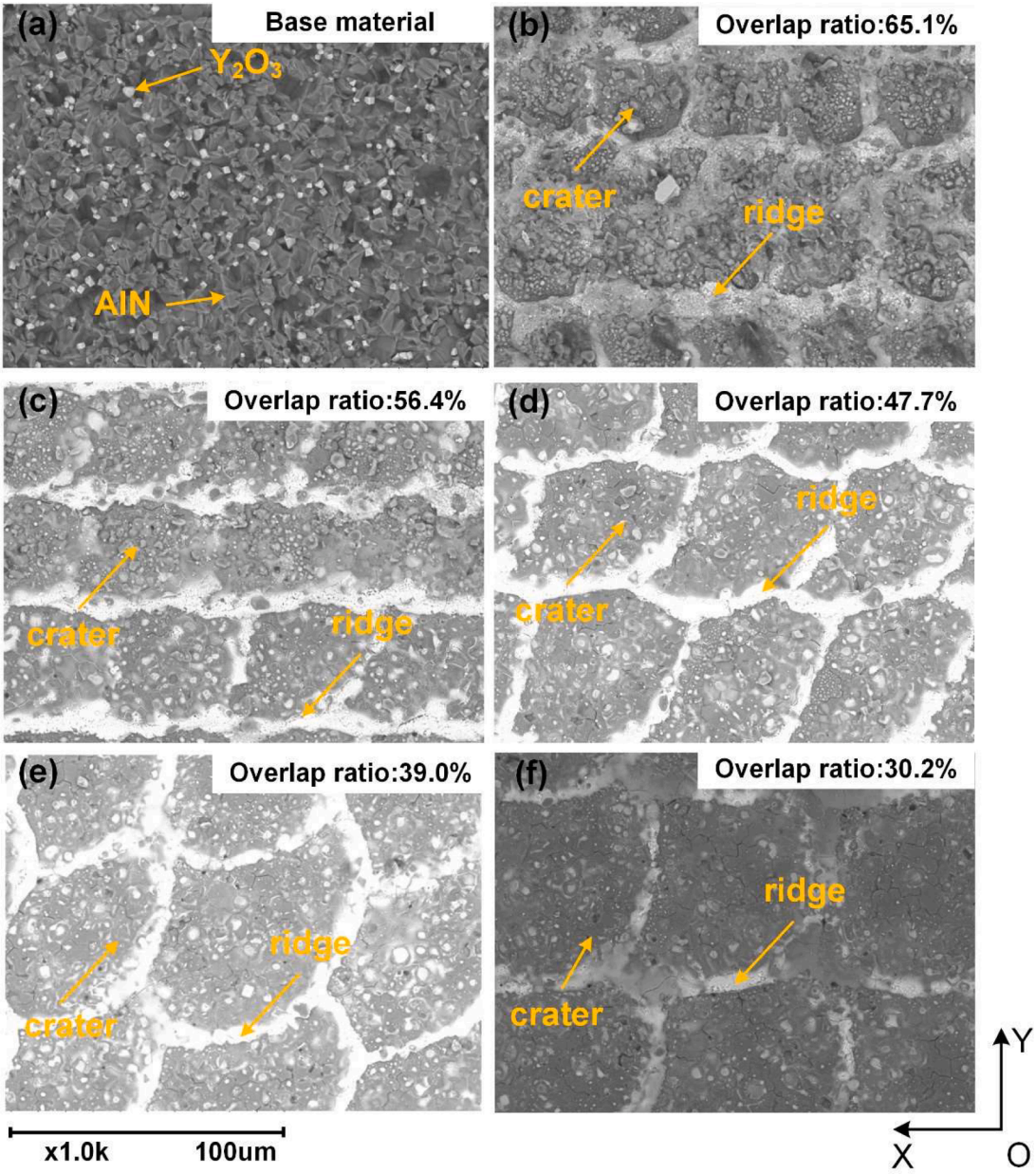

Fig. 9. The microstructure of laser-treated surfaces with 1000x magnification: (a) base material, (b) sample 3 with overlap ratio 65.1%, (c) sample 4 with overlap ratio of 56.4%, (d) sample 5 with overlap ratio of 47.7%, € sample 6 with overlap ratio of 39.0%, (f) sample 7 with overlap ratio of 30.2%.

the laser irradiation area as shown in Eq. 1 [33].

$$F = \frac{4P}{f\pi D^2} \tag{1}$$

Where F is the laser fluence (the average energy power density of the laser power spot), $P$is the laser power, f is the repetition frequency and D is the laser spot diameter.

Finally, the laser treatment parameters were set as follows: laser power (40 W), repetition frequency (5000 Hz), defocus diameter (+2.712 mm) and laser spot diameter D on the AlN plate surface was 97.5 μm. The laser fluence applied in the laser treatment F was 1.41 J/mm^2. The area of laser treatment on each sample was 8 mm × 8 mm.

Overlap ratios of laser pulses in X direction and Y direction were given in Eqs. 2 and 3, respectively [34,35].

$$O_x = \left(1 - \frac{V}{fD}\right) * 100\% \tag{2}$$

$$O_y = \left(1 - \frac{H}{D}\right) * 100\% \tag{3}$$

Where V is the laser scanning velocity, H is the hatch distance between adjacent laser scanning line in Y direction as shown in Fig. 1b.

The influence of the overlap ratio on surface metallization was studied in the present work. The overlap ratios in X direction and Y direction were set to the same in each experiment. The overlap ratios used in the experiment ranged from 30.2 % to 82.5 %. The experiment parameters were listed in Table. 1. As shown in Fig. 2a, when the overlap ratio was greater than 65.1 %, the laser-treated surface was ablated seriously. Only laser-treated surfaces with overlap ratios ranging from 65.1 % to 30.2 % (samples 3-7) were studied in the following sections. As shown in Fig. 2b, 3 samples were fabricated with each set of experiment parameters. The consistency of the macro-morphology of each laser-treated surface with the same set of experiment parameters indicated the process reproducibility. However, the black color of the laser-

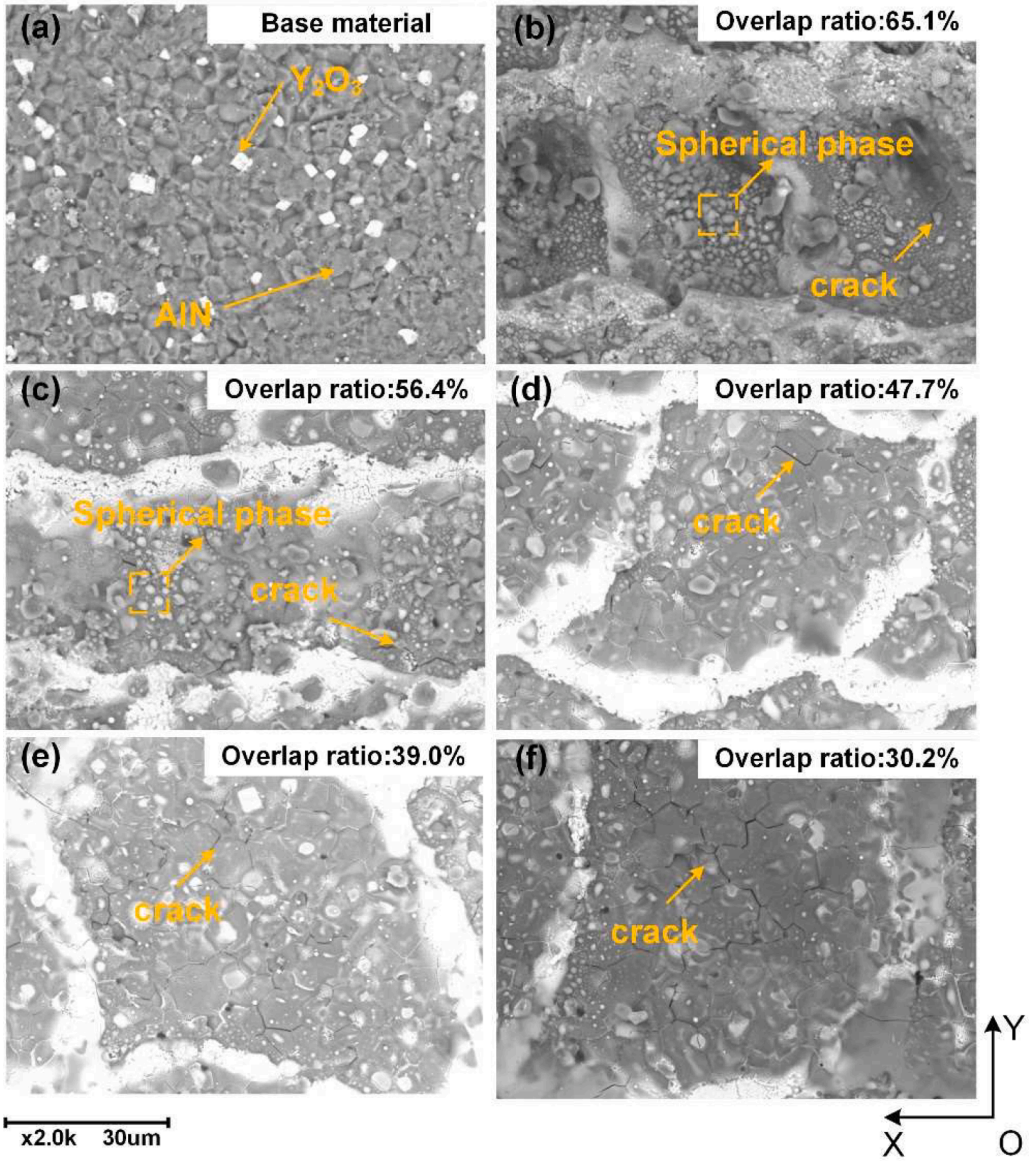

Fig. 10. The microstructure of laser-treated surfaces with 2000x magnification: (a) base material, (b) sample 3 with overlap ratio 65.1%, (c) sample 4 with overlap ratio of 56.4%, (d) sample 5 with overlap ratio of 47.7%, € sample 6 with overlap ratio of 39.0%, (f) sample 7 with overlap ratio of 30.2%.

treated surface with overlap ratio of 65.1 % indicated serious oxidation.

2.3. Measurement

After the laser treatment experiments, X-ray diffraction (Shimadzu XRD-7000) and Raman spectra tests (Renishaw Micro-Raman Spectroscopy System) were conducted to analyze the phase composition on the metallized surface. The digital microscope (EasyZoom5 3D) was applied to observe the cross-section morphology of laser-treated surface. The microstructure of laser-treated surface was observed with scanning electron microscopy equipped with EDX (SEM, Tescan VEGA3). The chemical composition of laser-treated surface was measured by EDX. The surface roughness in terms of Sa and Sz and processing depth were measured by the white light interferometer (WLI, Zygo NEXVIEW). The microstructure of unmetallized AlN surface was also observed by SEM. Finally, the hardness of metallized layer was measured by the nano-indenter (Agilent, G200).

3. Results and discussion

3.1. Phase composition after laser treatment

During laser treatment, the AlN samples were heated by laser. When the temperature of AlN ceramic exceeded the critical value, the AlN ceramic would decompose into Al and N_2. The decomposition mechanism could be expressed as [31]:

$$AlN(s) \rightarrow Al(s) + 1/2N_2(g), \Delta H = 3.13 \times 10^2 kJ/mol \quad (6)$$

Where (s), (l) and (g) denote the solid, liquid and gas phases, respectively. $\triangle H$. is the reaction enthalpy.

When the temperature reached 2573 K, the molten pool of Al would be formed on the AlN surface:

$$AlN(s) \rightarrow Al(l) + 1/2N_2(g), \Delta H = 3.23 \times 10^2 kJ/mol \quad (7)$$

When the temperature further reached 2767 K, the vaporization of Al would occur:

$$AlN(s) \rightarrow Al(g) + 1/2N_2(g), \Delta H = 6.43 \times 10^2 kJ/mol \quad (8)$$

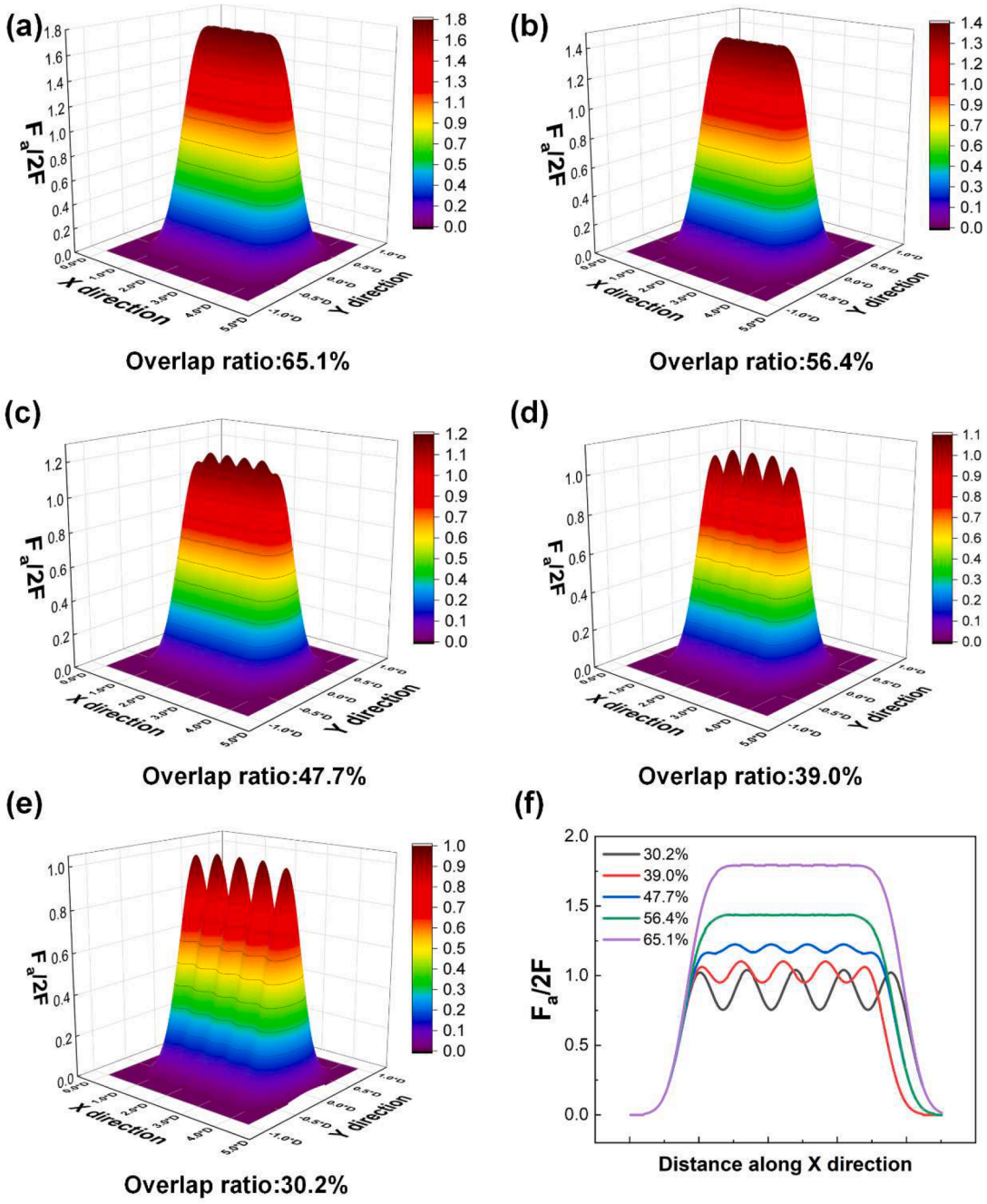

Fig. 11. The accumulated laser fluence in a single scanning line with different overlap ratios: (a) sample 3 with overlap ratio 65.1%, (b) sample 4 with overlap ratio of 56.4%, (c) sample 5 with overlap ratio of 47.7%, (d) sample 6 with overlap ratio of 39.0%, ϵ sample 7 with overlap ratio of 30.2%, (f) the accumulated laser fluence distribution along the symmetric axis.

The typical chemical composition of laser-treated surface (sample 3) was shown in Fig. 3. There were 2 kinds of phases formed on the surface. As shown in Fig. 3a, pure Al was formed. As shown in Fig. 3b-c, Al oxides were formed on the laser-treated surface.

The XRD result of AlN ceramic and the laser-treated surface were shown in Figs. 4 and 5, respectively. Besides AlN and Y_2O_3 (binder) in the base material, Al and Al_2O_3 were formed after laser treatment for samples 3–7 with overlap ratios ranging from 65.1 % to 30.2 %. Some compounds of Al and Y (such as Y_2Al and Y_5Al_3) were also formed on laser-treated surfaces.

The result of Raman spectrums was shown in Fig. 6. The three most intense peaks of Al-N bond in AlN ceramic (A_1(TO), E_2 and E_1(TO)) appeared in the Raman spectrum ofbase material [36,37]. However, it was found that these peaks decreased strongly after laser treatment. It indicated that the laser-treated surfaces were covered by an Al layer which gave a Raman spectrum without peak [29]. Besides, the peaks of samples 6 with overlap ratio of 39.0 % and 7 with overlap ratio of 30.2 % were higher than that of samples 3–5 with overlap ratio ranging from 65.1 % to 47.7 %. It demonstrated that the amount of decomposition product Al decreased with overlap ratio, which shielded the detection signal in the Raman spectrum test.

3.2. *Microstructure of metallized layer surface*

Fig. 7 showed the cross-section morphologies of laser-treated surfaces vertical to the laser scanning direction. All the laser-treated

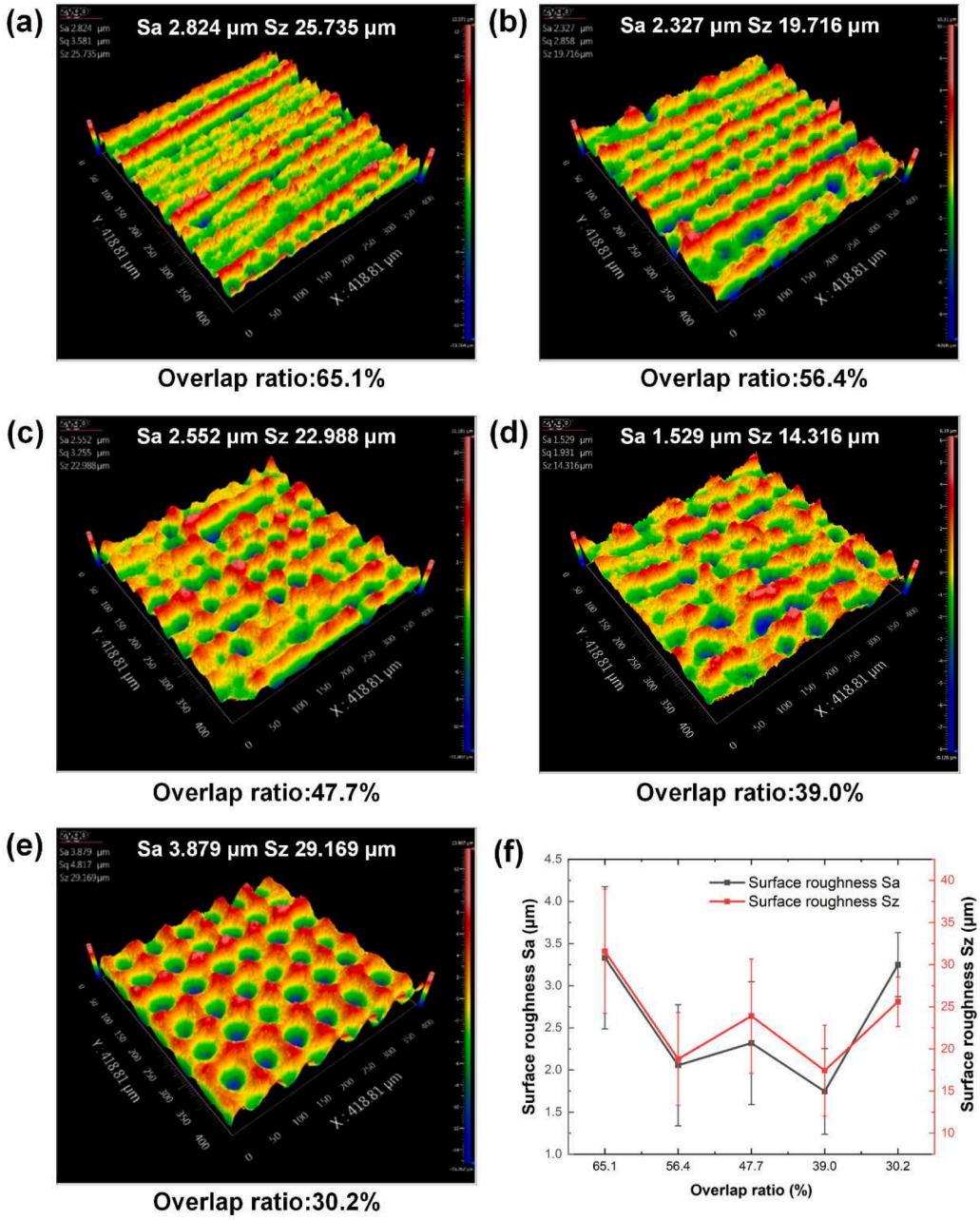

Fig. 12. The typical 3D surface topography of Al layer surfaces with different overlap ratios: (a) sample 3 with overlap ratio 65.1%, (b) sample 4 with overlap ratio of 56.4%, (c) sample 5 with overlap ratio of 47.7%, (d) sample 6 with overlap ratio of 39.0%, (e) sample 7 with overlap ratio of 30.2%, (f) the Sa values and Sz values of metallized layer surfaces with different overlap ratios.

surfaces were in a wave-shaped morphology. However, the wave-shaped morphologies of sample 3 with overlap ratio of 65.1 % and sample 4 with overlap ratio of 56.4 % were not very periodic. The microstructure at the wave-shaped morphology was shown in Fig. 8. Fig. 8a showed the cross-section microstructure of AlN ceramic, which was composed of AlN particles and Y_2O_3 particles. After laser treatment, Al was formed on the surface as shown in Fig. 8b.

Fig. 9a showed that the base material was consisted of AlN ceramic particles and Y_2O_3 polygonal phases. Fig. 9b-f showed the microstructure of Al layer on the AlN ceramic surface. It was found that the microstructure was consisted of a series of craters in a rectangular array, corresponding to the microstructural characteristic of metal laser treatment [38–40]. This phenomenon indicated that the surface microstructure resulted from the flow and solidification of molten Al, which was the AlN decomposition product. The shape of craters was circle, which was consistent with the shape of Gaussian laser spot. During the laser treatment, the subsequent laser remelted the ridge of the crater caused by preceding laser. A new ridge was formed by the subsequent laser. Therefore, the ridges stacked in both X direction and Y direction regularly. However, it was found that when the overlap ratio was higher than 47.7 % as shown in Fig. 9b and c, the ridge along Y direction was indistinct. It indicated that the molten pool caused by subsequent laser was formed before solidification of the molten pool caused by preceding laser. In this circumstance, the adjacent individual molten pools caused by individual laser spots merged into the consecutive molten pool. Fewer ridges were formed along Y direction.

Fig. 10 showed the detailed microstructure in the craters with 2000x magnification. There were spherical phases and cracks on the bottom of the craters. The spherical phases come from the condensation of the vaporized Al. The cracks resulted from the shrinkage of molten Al during

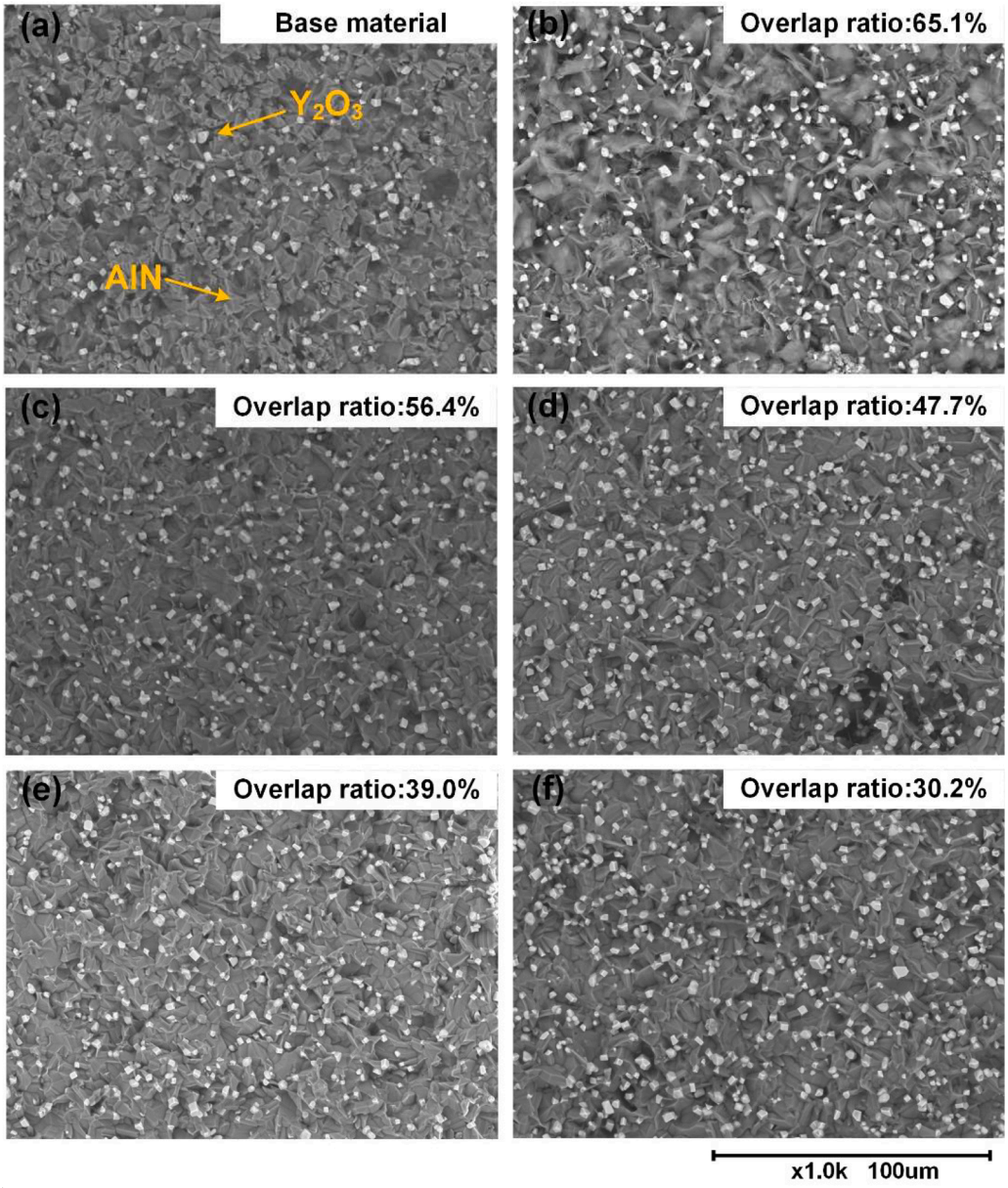

Fig. 13. The microstructure of unchanged AlN surface beneath Al layer with different overlap ratio with 1000x magnification: (a) base material, (b) sample 3 with overlap ratio 65.1%, (c) sample 4 with overlap ratio of 56.4%, (d) sample 5 with overlap ratio of 47.7%, (e) sample 6 with overlap ratio of 39.0%, (f) sample 7 with overlap ratio of 30.2%.

solidification. With the decrease of overlap ratio, it was found that the number of spherical phases decreased when the number of cracks increased.

To verify the key influence factor of metallized surface microstructure, the accumulated laser fluence in single laser scanning line (the sum of laser fluences accumulated by different lasers at the same point in single laser scanning line) was determined, as shown in Fig. 11 (The unit of both X and Y axis was the laser spot diameter D). The accumulated laser fluence distribution was shown in Fig. 11a-e. It was found that when the overlap ratio was greater than 47.7 %, the fluctuation of accumulated laser fluence along laser scanning direction was very small. When the overlap ratio was equal to or smaller than 47.7 %, the periodic peak value and valley value of accumulated laser fluence were formed. The accumulated laser fluence along the symmetric axis of single laser scanning line was shown in Fig. 11f. It was seen that the peak value of accumulated laser fluence increased from 2.93 J/mm^2 to 5.06 J/mm^2 when overlap ratio increased from 30.2 % to 65.1 %. The accumulated laser fluence value and consistency along laser scanning direction decreased with overlap ratio.

With great value and high consistency of accumulated laser fluence along laser scanning direction, the consecutive molten pool was formed. With small value and low consistency of accumulated laser fluence along laser scanning direction, individual molten pools were formed. The ridges along Y direction were formed as shown in Fig. 9d-f. Besides, the amount of vaporized and molten Al decreased with accumulated laser fluence. Therefore, a large amount of Al was vaporized and then congealed on the Al surface to form spherical phases with great overlap ratios (65.1 % and 56.4 %) as shown in Fig. 10b and c. However, with small overlap ratios (47.7 %, 39.0 % and 30.2 %), small amount of vaporized and molten Al was generated. Therefore, little condensation of vaporized Al occurred. No spherical phase was formed. Besides, the amount of molten Al was too small. Many gaps were formed during solidification of molten Al. No molten Al flowed into the gaps due to the shrinkage of Al for compensation. Finally, numerous cracks were formed

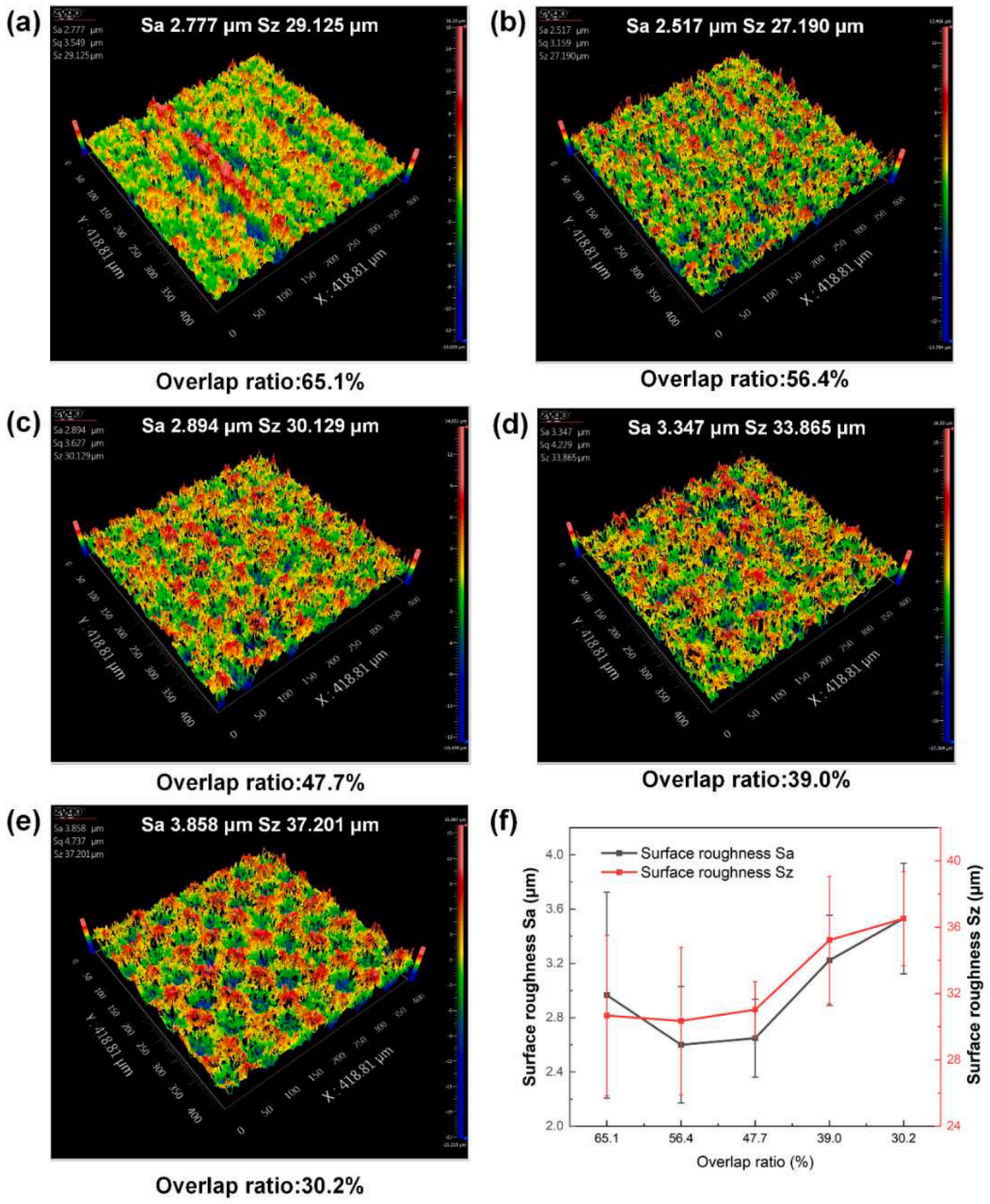

Fig. 14. The typical 3D surface topographies of unmetallized layers with different overlap ratios: (a) sample 3 with overlap ratio 65.1%, (b) sample 4 with overlap ratio of 56.4%, (c) sample 5 with overlap ratio of 47.7%, (d) sample 6 with overlap ratio of 39.0%, (e) sample 7 with overlap ratio of 30.2%, (f) the Sa values and Sz values of unmetallized surfaces with different overlap ratios.

with small overlap ratios as shown in Fig. 10d-f.

Besides, the flow behavior in the consecutive molten pool was fiercer than that in individual molten pool due to higher absorbed laser energy. Therefore, the cross-section morphologies of sample 3 with overlap ratio of 65.1 % and sample 4 with overlap ratio of 56.4 % for each laser path were more irregular. In this circumstance, the wave-shaped morphologies of sample 3 with overlap ratio of 65.1 % and sample 4 with overlap ratio of 56.4 % were not very periodic as shown in Fig. 7a-b.

3.3. *Surface roughness of metallized layer surface*

The typical three-dimensional (3D) surface topography and surface roughness after laser treatment with different overlap ratios were shown in Fig. 12. With overlap ratio greater than 47.7 % as shown in Fig. 12a-b, the ridges were only formed along X direction. The phenomenon was consistent with the microstructure of metallized layer surface. The consecutive molten pool was formed along X direction. Therefore, fewer ridges were formed along Y direction. In addition, the time interval of adjacent laser spot overlapping along Y direction was at least 23.5 ms (=distance/greatest laser scanning velocity). This value was much greater than the molten pool solidification time. Therefore, in Y direction, the molten pool caused by preceding laser solidified before the molten pool caused by subsequent laser was formed. In this circumstance, ridges along X direction were formed by each laser spot.

With an overlap ratio equal to or smaller than 47.7 % as shown in Fig. 12c-e, individual molten pools in both X and Y direction were formed. The ridges were formed in both X and Y directions. The surface roughness of the Al layer surface was obtained by measuring 5 areas of each specimen. The average values and standard deviations of surface roughness of the laser-treated surfaces with different overlap ratios were shown in Fig. 12f. It was found that with the same molten pool mode (consecutive molten pool for sample 3 with overlap ratio of 65.1 %and

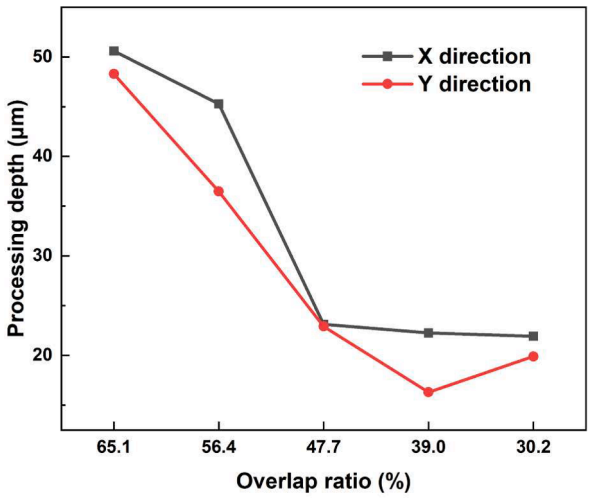

Fig. 15. The processing depths with different overlap ratios.

sample 4 with overlap ratio of 56.4 % or individual molten pool for sample 5 with overlap ratio of 47.7 % and sample 6 with overlap ratio of 39.0 %), the surface roughness Sa and Sz decreased with overlap ratio. It could be seen from Fig. 2a-b that the process effect of sample 7 with overlap ratio of 30.2 % was not homogenous. Therefore, the surface roughness increased dramatically.

3.4. Microstructure of unmetallized AlN surface

In order to measure the microstructure, surface roughness and thickness of metallized layer, the metallized layer on the AlN surface was required to be removed. The chemical etching was applied. The laser-treated samples were placed in NaOH solution (solute concentration was 43 mg/ml). The chemical bath for each sample was carried out at the temperature of 45 °C for 4 hours. Al and Al_2O_3 reacted with hydroxyl ion [41,42]. The Al and Al_2O_3 were translated into meta-aluminate which dissolved in water as illustrated in Eqs. 9 and 10. After the chemical etching, the generated Al layer and the oxidation of Al was removed.

$$2Al + 2NaOH + 2H_2O \rightarrow 2NaAlO_2 + H_2O \quad (9)$$

$$Al_2O_3 + 2NaOH \rightarrow 2NaAlO_2 + H_2O \quad (10)$$

The microstructure of unmetallized AlN surface beneath the metallized layer was observed as shown in Fig. 13 (with 1000 × magnification). Compared to the microstructure of base material in Fig. 13a, the smooth areas observed on the unmetallized surface indicated the slight melting of AlN in Fig. 13b. The melting point of AlN ceramic was 3000 K [42,43]. It was found that the slight melting of AlN was only observed with overlap ratio 65.1 % for greatest accumulated laser fluence in Fig. 11. No crack was found on the unmetallized AlN surface, indicated no damage was induced to the unmetallized AlN ceramic.

3.5. Surface roughness of unmetallized surface

The typical 3-D surface topographies of unmetallized AlN surfaces with different overlap ratios were shown in Fig. 14. Compared to Fig. 12, the characteristic of surface topography of unmetallized AlN surfaces was different from that of metallized layer surface. With an overlap ratio greater than 47.7 % as shown in Fig. 14a-b, few ridges were formed along Y direction. Besides, the small local fluctuation of surface topography of unmetallized AlN surface was more apparent than that of metallized layer. The surface topographies of unmetallized surfaces were seen to be coarser. The surface roughness of unmetallized surface were obtained by measuring 5 areas of each sample. The average values and standard deviations of surface roughness with different overlap ratios were shown in Fig. 14f. It was found that the surface roughness increased when overlap ratio decreased from 56.4 % to 30.2 %. The smallest Sa and Sz of unchanged AlN surface was 2.6 μm and 30.4 μm respectively with overlap ratio of 56.4 %. The surface roughness with an overlap ratio of 65.1 % was greater than that with 56.4 %, which may be caused by the serious oxidation.

3.6. Processing depth

The average height difference of AlN original surface and the unmetallized surface beneath the metallized layer was measured by WLI, which was defined as the processing depth.

The processing depths with different overlap ratios were shown in Fig. 15. It was found that the processing depth along X direction was higher than the processing depth along Y direction. It was related to the difference between the time intervals of adjacent laser spot overlapping along X and Y direction. Along X direction, the time interval of adjacent

Table 2
The hardness values of test points in the nanoindentation test.

	Hardness (Point 1)	Hardness (Point 2)	Hardness (Point 3)	Hardness (Point 4)	Average hardness
Specimen 3	0.83 GPa	0.83 GPa	0.60 GPa	0.69 GPa	0.738 GPa
Specimen 4	0.71 GPa	0.71 GPa	0.72 GPa	0.69 GPa	0.708 GPa

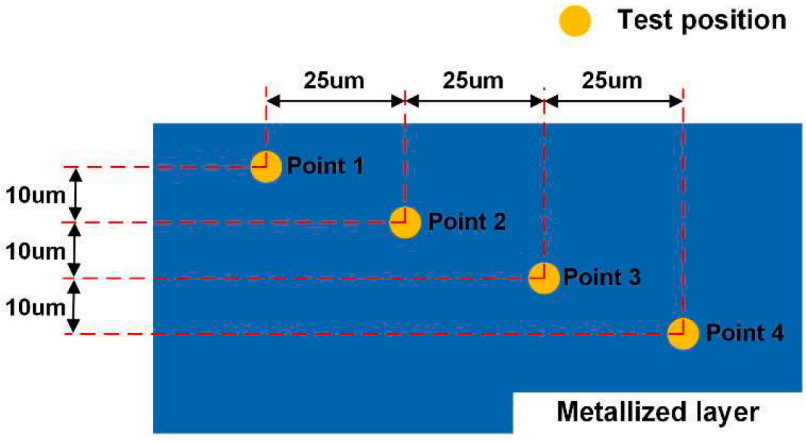

Fig. 16. The positions of test points in the nanoindentation test.

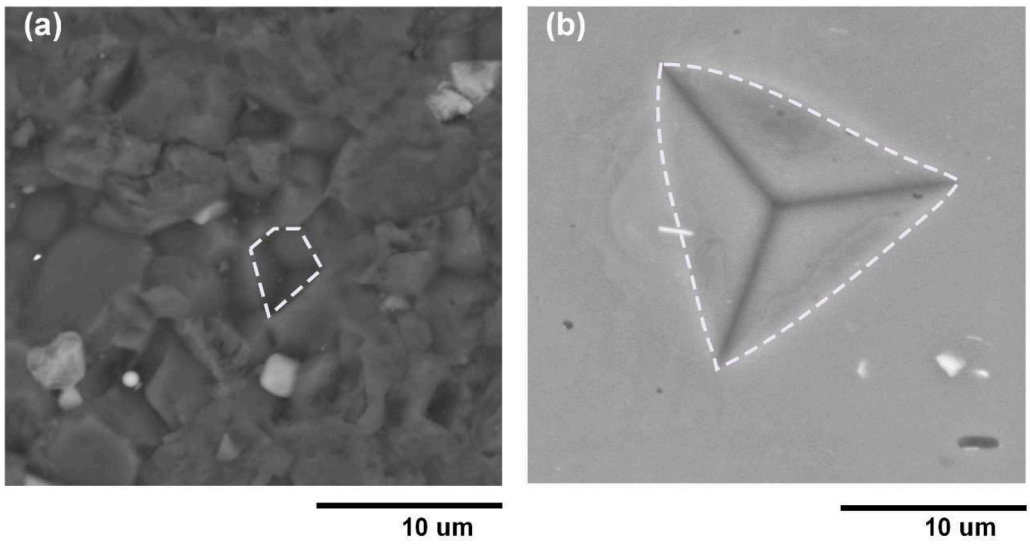

Fig. 17. The residual indentation morphologies of: (a) AlN ceramic, (b) metallized layer.

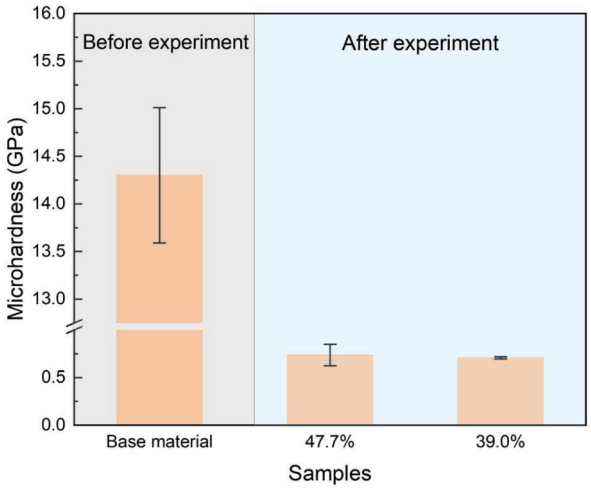

Fig. 18. Comparison between base material hardness and metallized layer hardness.

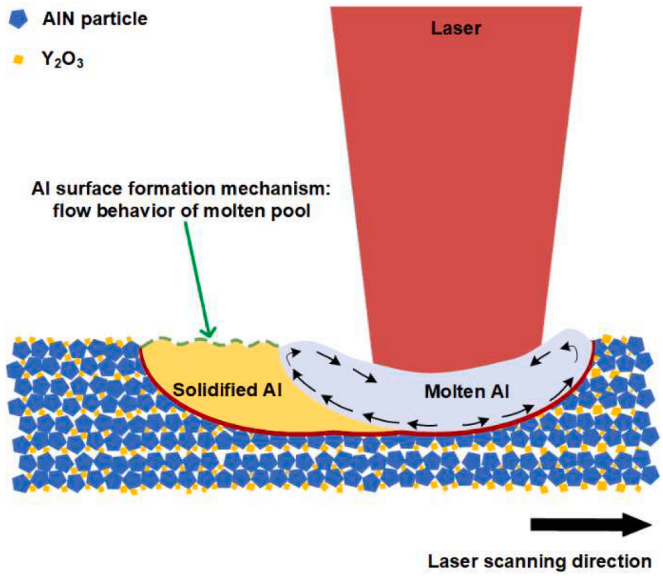

Fig. 19. The formation mechanism of Al layer surface.

laser spot overlapping was 0.2 ms (=1 s/repetition frequency). However, the time interval of adjacent laser spot overlapping in Y direction was greater than 23.5 ms (=distance/greatest laser scanning velocity) as mentioned in Section 3.3. When the absorbed energies from 2 adjacent laser spots was the same, the energy dissipation time between adjacent laser pulse along Y direction was much longer than that along X direction. It caused the energy accumulation along X direction to be greater than that along Y direction. Therefore, the processing depth along X direction was greater than that along Y direction. This phenomenon indicated that the processing depth was not only related to the overlap ratio in spatial domain but also the time interval of adjacent laser spot overlapping in time domain.

The processing depths of sample 3 with overlap ratio 65.1 % and sample 4 with overlap ratio 56.4 %were apparently greater than that of samples 5–7 with overlap ratio ranging from 47.7 % to 30.2 %. The processing depth was influenced by the depth of molten pool. Since more accumulated laser fluence was absorbed by the consecutive molten pool, the size of consecutive molten pool with overlap ratios of 65.1 % and 56.4 % for sample 3 and sample 4 was greater than the size of the individual molten pool with overlap ratios of 47.7 %, 39.0 % and 30.2 % for samples 5–7. Therefore, processing depths of sample 3 and sample 4 were apparently greater than that of samples 5–7. Besides, the processing depth of samples 5–7 were similar due to the same individual molten pool mode and similar accumulated laser fluence.

3.7. Hardness variation after laser treatment

To evaluate the surface softening degree, a nanoindentation test was conducted on the cross section of metallized layer. In order to guarantee the reliability of measurement, the hardness of 4 positions in the metallized layer was measured as shown in Fig. 16. The distance between adjacent points along horizontal direction and vertical direction were set as 25 μm and 10 μm respectively to ensure the independence of measurement result of each test point. The nanoindentation test area range was 75 μm (along horizontal direction) × 30 μm (along vertical direction). The constant load mode was applied in the nanoindentation test. In each test, the load was 300 μN. The load time was 10 s. The holding time was 2 s. The unloading time was 10 s. Due to the processing depths of samples 5-7 with overlap ratios ranging from 47.7 % to 30.2 % were less than 30 μm, which did not satisfy the requirement of

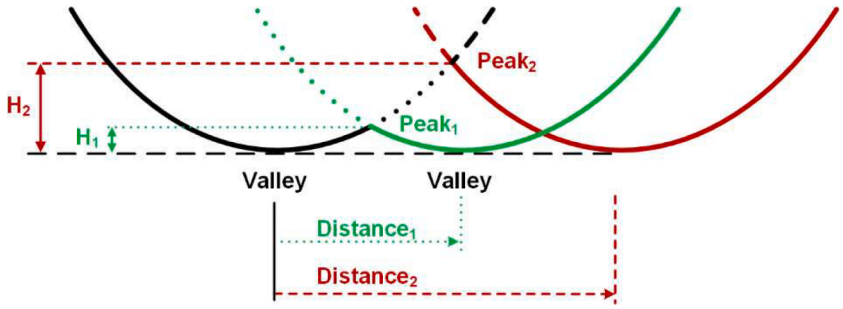

Fig. 20. The formation mechanism of unmetallized AlN surface.

nanoindentation test, only samples 3 with overlap ratio of 65.1 % and 4 with overlap ratio of 56.4 % were used in the indentation test.

The hardness values of test points were shown in Table. 2. The average metallized layer hardness of sample 3 with overlap ratio 65.1 % was 0.738 GPa, while metallized layer hardness of sample 4 with overlap ratio of 56.4 % was 0.708 GPa. These values were close to the aluminum hardness value [44]. The hardness of base material was also measured. The average hardness value of AlN ceramic was 14.3 GPa. The characteristic residual indentation morphologies of AlN ceramic and metallized layer were shown in Fig. 17. By comparing the hardness values of metallized layer and base material as shown in Fig. 18, it was concluded that surface softening was achieved by laser treatment.

4. Discussion

From the comparison of experimental results, it was found that both the microstructure and surface roughness of surface softened layer and unmetallized layer were different. All the differences were caused by the different formation mechanisms of softened surface layer and unmetallized surface.

It was concluded that during the laser treatment, a molten pool composed of molten Al was generated on the surface as shown in Fig. 19. With a great overlap ratio (65.1 % and 56.4 %), a consecutive molten pool was formed. With low overlap ratio (47.7 %, 39.0 % and 30.2 %), an individual molten pool was formed. The surface topography was controlled by the molten pool flow behavior. In the same molten pool mode, with the decrease of overlap ratio in X direction, energy absorbed by the molten pool decreased. Therefore, the molten Al temperature decreased, which led to the increase of molten Al viscosity and the decrease of molten Al amount. In this circumstance, the flow behavior was more stable with greater laser scanning velocity for the same kind of molten pool (consecutive molten pool and individual molten pool). It could be observed from Fig. 10 that the surface roughness of sample 4 with overlap ratio of 56.4 % was lower than that of sample 3 with overlap ratio of 65.1 %. Besides, the surface roughness of sample 6 with overlap ratio of 39.0 % was lower than that of sample 5 with overlap ratio of 47.7 %. Furthermore, the surface roughness of sample 7 with overlap ratio 30.2 % increased dramatically due to the processing heterogeneity as shown in Fig. 2a-b.

The unmetallized AlN surface topography was controlled by the AlN decomposition reaction. During the laser treatment experiment, AlN decomposed into Al and N_2. AlN particles completely decomposed or partially decomposed. Because the AlN particle size (less than 3 μm) was much smaller laser irradiation area size (diameter: 97.5 μm), the influence of AlN particle size could be ignored. The influence of overlap ratio on unchanged AlN surface topography was shown in Fig. 20. The arcs represented the boundary between the decomposition reaction area and base material. The surface peak and valley were formed by the overlapping between adjacent decomposition reaction area. When the overlap ratio decreased, the distance between two individual decomposition reaction area increased (from $Distance_1$ to $Distance_2$). The height difference between peak to valley increased (from H_1 to H_2). Therefore, the surface roughness increased with decreasing of overlap ratio as shown in Fig. 14. However, the surface roughness of unchanged AlN surface with overlap ratio of 65.1 % was a little greater than that with overlap ratio of 56.4 %. It was speculated that this phenomenon was caused by the slight melting of AlN particle shown in Fig. 13a.

5. Conclusion

To reveal surface softening mechanism of Aluminum Nitride (AlN) ceramic by laser irradiation, microsecond pulse laser was applied to soften the AlN ceramic surface. The influence of overlap ratio on surface softening was investigated. The microstructures of surface softened layer and unchanged AlN surface were observed. To evaluate the improvement of machinability, the surface hardness and surface roughness were measured. The main conclusions were as following:

(1) With overlap ratio of 56.4 %, relatively thick metallized layer with relatively small surface roughness on the AlN ceramic surface can be obtained by laser treatment. The thicknesses of metallized layer were 45.3 μm in X direction and 36.5 μm in Y direction, respectively. The surface roughness Sa was 2.3 μm. The surface roughness Sz was 19.7 μm.
(2) Al and Aluminum Oxide (Al_2O_3) were formed on the laser-treated surface; The number of cracks on the surface increased with the decreasing of overlap ratio.
(3) Both accumulated laser fluence distribution in spatial domain and time interval between laser pulse in time domain affected the microstructure and surface roughness significantly.
(4) The surface roughness of metallized surface was affected by flow behavior of molten Al while the surface roughness of unmetallized surface was affected by the overlap ratio of decomposition craters.
(5) The molten pool mode (consecutive/individual) affected the processing depth significantly. The processing depth with consecutive molten pool was greater due to the greater accumulated laser fluence.
(6) The hardness of AlN ceramic surface decreased from 14.3 GPa to 0.708 GPa after metallization by laser treatment.

The hardness of AlN ceramic surface decreased after laser treatment. However, the surface roughness increased compared to base material. The change of machinability of the laser-treated AlN needs to be further verified by the ultra-precision machining experiment. Our next goal is to investigate the comprehensive effect of hardness and surface roughness of laser-treated AlN surface on the machinability of AlN ceramic in machining experiment.

CRediT authorship contribution statement

Lingda Xiong: Writing – original draft, Investigation, Formal analysis. **Chunjin Wang:** Writing – review & editing, Supervision, Resources, Methodology, Conceptualization. **Wei Wu:** Investigation.

Linjiang Xu: Data curation. **Chunming Wang:** Resources. **Hui Deng:** Writing – review & editing, Resources. **Chi Fai Cheung:** Writing – review & editing, Supervision, Resources.

Declaration of competing interest

The authors declare that they have no known competing financial interests or personal relationships that could have appeared to influence the work reported in this paper.

Data availability

Data will be made available on request.

Acknowledgement

This work was mainly supported by the Shenzhen-Hong Kong-Macau Technology Research Programme (Project No: SGDX20220530110804030), the Innovation and Technology Commission (ITC) of the Government of the Hong Kong Special Administrative Region (HKSAR), China (GHP/142/19SZ), and the Research and Innovation Office of The Hong Kong Polytechnic University (Project code: BD9B). We would also like to express our gratitude to the Analysis and Test Center of Huazhong University of Science and Technology (HUST) and the State Key Laboratory of Digital Manufacturing Equipment & Technology of HUST for their friendly cooperation.

References

[1] P.A.M. Aguilar, M. Vlasova, M. Kakazey, D.M. Cruz, E.J. Arellano, V. Stetsenko, T. Tomila, A. Ragulya, Features of formation of channels during laser treatment of AlN ceramics, Opt. Laser. Technol. 42 (2010) 172–179.
[2] J. Shao, H. Dong, R.L. Zhang, Y.M. Wang, S.L. Han, Effect of laser parameters and atmosphere in the structuring of aluminum nitride, Int. J. Appl. Ceram. Technol. 19 (2022) 3040–3048.
[3] H.Y. Zheng, H.M. Phillips, J.L. Tan, G.C. Lim, Laser-induced conductivity in aluminum nitride, P. Soc. Photo-Opt. Ins. 3898 (1999) 280–286.
[4] J. Kaur, N. Kuwano, K.R. Jamaludin, M. Mitsuhara, H. Saito, S. Hata, S. Suzuki, H. Miyake, K. Hiramatsu, H. Fukuyama, Electron microscopy analysis of microstructure of postannealed aluminum nitride template, Appl. Phys. Express. 9 (2016).
[5] H.G. Li, R.K. Kang, S. Gao, X.L. Zhu, Surface damage characteristics of AlN ceramics induced by ultra-precision grinding, Mater. Manuf. Process. 37 (2022) 1610–1617.
[6] A. Rashid, A. Bilal, C. Liu, M.P. Jahan, D. Talamona, A. Perveen, Effect of conductive coatings on micro-electro-discharge machinability of aluminum nitride ceramic using on-machine-fabricated microelectrodes, Materials 12 (2019).
[7] W.S. Cho, M.W. Cho, J.H. Lee, Z.A. Munir, Effects of h-BN additive on the microstructure and mechanical properties of AlN-based machinable ceramics, Mat. Sci. Eng. a-Struct. 418 (2006) 61–67.
[8] A. Bilal, A. Rashid, C. Liu, M.P. Jahan, D. Talamona, A. Perveen, Powder mixed micro electro discharge machining of aluminium nitride ceramic. Matec Web Conf, 2019, p. 303.
[9] G.L. Zhao, Z.W. Nian, Z.H. Zhang, L. Li, N. He, Enhancing the machinability of Cf/SiC composite with the assistance of laser-induced oxidation during milling, J. Mater. Res. Technol. 22 (2023) 1651–1663.
[10] G.L. Zhao, L.J. Xin, L. Li, Y. Zhang, N. He, H.N. Hansen, Cutting force model and damage formation mechanism in milling of 70wt% Si/Al composite, Chin. J. Aeronaut. 36 (2023) 114–128.
[11] J.G. Zhang, Y.F. Fu, X. Chen, Z.F. Shen, J.J. Zhang, J.F. Xiao, J.F. Xu, Investigation of the material removal process in in-situ laser-assisted diamond cutting of reaction-bonded silicon carbide, J. Eur. Ceram. Soc. 43 (2023) 2354–2365.
[12] H. Deng, K. Endo, K. Yamamura, Competition between surface modification and abrasive polishing: a method of controlling the surface atomic structure of 4H-SiC (0001), Sci. Rep.-Uk 5 (2015).
[13] K.Y. You, F.Z. Fang, High effective laser assisted diamond turning of binderless tungsten carbide, J. Mater. Process Tech. 302 (2022).
[14] C.W. Cao, Y.B. Feng, T. Qiu, J. Yang, X.Y. Li, T. Liang, J. Li, Effects of isothermal annealing on the oxidation behavior, mechanical and thermal properties of AlN ceramics, Ceram. Int. 43 (2017) 9334–9342.
[15] Z.Q. Zhou, X.M. Chen, Y. Yuan, L. Shi, W.L. Jiang, B. Yang, B.Q. Xu, D.C. Liu, A comparison of the thermal decomposition mechanism of wurtzite AlN and zinc blende AlN, J. Mater. Sci. 53 (2018) 11216–11227.
[16] P.M. Dryburgh, The estimation of maximum growth-rate for aluminum nitride crystals grown by direct sublimation, J. Cryst. Growth 125 (1992) 65–68.
[17] M.V. Averyanova, I.N. Przhevalskii, S.Y. Karpov, Y.N. Makarov, M.S. Ramm, R. A. Talalaev, Analysis of vaporization kinetics of group-III nitrides, Mat. Sci. Eng. B-Solid 43 (1997) 167–171.
[18] L.J. Zhao, J. Cheng, M.J. Chen, X.D. Yuan, W. Liao, Q. Liu, H. Yang, H.J. Wang, Formation mechanism of a smooth, defect-free surface of fused silica optics using rapid CO2 laser polishing, Int. J. Extreme Manuf. 1 (2019).
[19] G.D. Zhu, Z.H. Xu, Y. Jin, X. Chen, L.J. Yang, J. Xu, D.B. Shan, Y.B. Chen, B. Guo, Mechanism and application of laser cleaning: a review, Opt. Laser Eng. 157 (2022).
[20] L.Z. Wang, W.Q. Zhao, X.S. Mei, Z.X. Yang, X.W. Shen, H.D. Liu, Improving quality and machining efficiency of hole during AlN trepanning with nanosecond pulse laser, Ceram. Int. 46 (2020) 24018–24028.
[21] T. Primus, L. Beranek, Z. Pitrmuc, J. Simota, P. Zeman, Laser polishing of additively manufactured 316L stainless steel with different construction angles, Int. J. Adv. Manuf. Tech. 121 (2022) 3215–3228.
[22] B. Wang, X.C. Wang, H.Y. Zheng, Y.C. Lam, Surface wettability modification of cyclic olefin polymer by direct femtosecond laser irradiation, Nanomaterials-Basel 5 (2015) 1442–1453.
[23] F. Dong, R. Li, G. Wu, K. Liang, G.L. Li, Y.T. Nie, Z.Y. Gan, Q. Cao, X.H. Wang, Q. Z. Zhao, S. Liu, An investigation of aluminum nitride thin films patterned by femtosecond laser, Appl. Phys. Lett. 116 (2020).
[24] W. Kautek, P. Rudolph, G. Daminelli, J. Kruger, Physico-chemical aspects of femtosecond-pulse-laser-induced surface nanostructures, Appl. Phys. a-Mater. 81 (2005) 65–70.
[25] S.H. Kim, I.B. Sohn, S. Jeong, Ablation characteristics of aluminum oxide and nitride ceramics during femtosecond laser micromachining, Appl. Surf. Sci. 255 (2009) 9717–9720.
[26] Y. Hirayama, H. Yabe, M. Obara, Selective ablation of AlN ceramic using femtosecond, nanosecond, and microsecond pulsed laser, J. Appl. Phys. 89 (2001) 2943–2949.
[27] N. Nedyalkov, A. Dikovska, L. Aleksandrov, M. Terakawa, Nanosecond laser ablation of AlN ceramic, Appl. Phys. a-Mater. 127 (2021).
[28] Q.B. Yang, Y. Chen, Z.H. Lv, L. Chen, D.Y. Lou, Z. Zheng, J. Cheng, D. Liu, Nanosecond laser surface processing of AlN ceramics, J. Mater. Sci. 54 (2019) 13874–13882.
[29] G. Nicolas, M. Autric, Production of a metallic thin film on AlN surface by UV laser radiation, Appl. Surf. Sci. 109 (1997) 477–481.
[30] G. Nicolas, G. Vacquier, M. Autric, L. Yaghdjian, Characterization of modifications observed on nitrides after an UV laser exposure, Appl. Surf. Sci. 138 (1999) 538–542.
[31] J. Shao, R.L. Zhang, S.L. Han, H. Dong, S.F. Sun, The activation threshold evaluation of metallization for aluminum nitride ceramic under nanosecond laser pulses in air, Ceram. Int. 47 (2021) 24707–24712.
[32] B. Stolz, R. Poprawe, Surface conductivity modification of ceramics with laser radiation, Surf. Coat. Tech. 112 (1999) 394–400.
[33] A. Temmler, D. Liu, J. Luo, R. Poprawe, Influence of pulse duration and pulse frequency on micro-roughness for laser micro polishing (L mu P) of stainless steel AISI 410, Appl. Surf. Sci. 510 (2020).
[34] D. Bhaduri, P. Penchev, A. Batal, S. Dimov, S.L. Soo, S. Sten, U. Harrysson, Z. X. Zhang, H.S. Dong, Laser polishing of 3D printed mesoscale components, Appl. Surf. Sci. 405 (2017) 29–46.
[35] J. Sabbaghzadeh, M.J. Hamedi, F.M. Ghaini, M.J. Torkamany, Effect of process parameters on the melting ratio in overlap pulsed laser welding, Metall. Mater. Trans. B 39 (2008) 340–347.
[36] E. Radhika, T. Samuel, P. Dobbidi, A modified sintering method to prepare phase pure AlN ceramics: structural and dielectric studies for microwave applications, Ceram. Int. 48 (2022) 29372–29385.
[37] Y.L. He, H.M. Wu, Investigation on low-temperature sintered AlN nanoceramics with high thermal conductivity, Int. J. Appl. Ceram. Tech. 16 (2019) 2101–2106.
[38] B.W. Liu, C.M. Wang, G.Y. Mi, Simulation of the removal mechanism of thermo-oxidized layer and surface morphological evolution on TA15 alloy under nanosecond pulsed laser ablation by multiphase flow model, J. Manuf. Process. 69 (2021) 69–83.
[39] Y.L. Zhang, Q. Yao, W.F. Long, C.M. Wang, J. Lin, Z.H. Liu, Welding defect and mechanical properties of nanosecond laser cleaning 6005A aluminum alloy, Materials 15 (2022).
[40] J. Lin, C.M. Wang, A study of surface quality and mechanical strength in 5083 aluminum alloy plates using pulsed laser cleaning, J. Mech. Sci. Technol. 36 (2022) 5223–5229.
[41] P.E. Koziol, A.J. Antonczak, P. Szymczyk, B. Stepak, K.M. Abramski, Conductive aluminum line formation on aluminum nitride surface by infrared nanosecond laser, Appl. Surf. Sci. 287 (2013) 165–171.
[42] A.J. Antonczak, P.E. Koziol, B. Stepak, P. Szymczyk, K.M. Abramski, Direct selective metallization of AlN ceramics induced by laser radiation, Proc. Spie 8968 (2014).
[43] L.G. D'yachkov, L.A. Zhilyakov, A.V. Kostanovskii, Melting of aluminum nitride at atmospheric nitrogen pressure, Tech. Phys+ 45 (2000) 928–930.
[44] T.T. Zhang, W.X. Wang, J. Zhou, X.Q. Cao, Z.F. Yan, Y. Wei, W. Zhang, Investigation of interface bonding mechanism of an explosively welded tri-metal titanium/aluminum/magnesium plate by nanoindentation, Jom-Us 70 (2018) 504–509.